OXFORD

ORIGINAL ARTICLE

Genetic ablation of IP$_3$ receptor 2 increases cytokines and decreases survival of SOD1^{G93A} mice

Kim A. Staats[1,2], Stephanie Humblet-Baron[3], Andre Bento-Abreu[1,2],
Wendy Scheveneels[1,2], Alexandros Nikolaou[4,5,6], Kato Deckers[7],
Robin Lemmens[1,2,8], An Goris[9], Jo A. Van Ginderachter[5,6],
Philip Van Damme[1,2,8], Chihiro Hisatsune[10], Katsuhiko Mikoshiba[10],
Adrian Liston[3], Wim Robberecht[1,2,8] and Ludo Van Den Bosch[1,2,*]

[1]KU Leuven - University of Leuven, Department of Neurosciences, Experimental Neurology and Leuven
Research Institute for Neuroscience and Disease (LIND), [2]VIB, Vesalius Research Center, Laboratory of
Neurobiology, [3]VIB and Department of Microbiology and Immunology, KU Leuven, Leuven, Belgium,
[4]Molecular and Biochemical Pharmacology Laboratory, Vrije Universiteit Brussel, [5]Myeloid Cell Immunology
Laboratory, VIB, Inflammation Research Center, [6]Cellular and Molecular Immunology Unit, Vrije Universiteit
Brussel, Brussels, Belgium, [7]Center for Molecular and Vascular Biology, University of Leuven, [8]University
Hospitals Leuven, Department of Neurology, [9]KU Leuven - University of Leuven, Department of Neurosciences,
Laboratory for Neuroimmunology, Leuven, Belgium and [10]Laboratory for Developmental Neurobiology, Brain
Science Institute, RIKEN, Wako-shi, Saitama, Japan

*To whom correspondence should be addressed at: L. Van Den Bosch, Neurobiology, Campus Gasthuisberg O&N4 PB 912, Herestraat 49, B-3000 Leuven,
Belgium. Tel: +32 16 330681; Fax: +32 16 372534; E-mail: ludo.vandenbosch@vib-kuleuven.be

Abstract

Amyotrophic lateral sclerosis (ALS) is a devastating progressive neurodegenerative disease characterized by the selective
death of motor neurons. Disease pathophysiology is complex and not yet fully understood. Higher gene expression of the
inositol 1,4,5-trisphosphate receptor 2 gene (*ITPR2*), encoding the IP$_3$ receptor 2 (*IP$_3$R2*), was detected in sporadic ALS patients.
Here, we demonstrate that *IP$_3$R2* gene expression was also increased in spinal cords of ALS mice. Moreover, an increase of
IP$_3$R2 expression was observed in other models of chronic and acute neurodegeneration. Upregulation of *IP$_3$R2* gene
expression could be induced by lipopolysaccharide (LPS) in murine astrocytes, murine macrophages and human fibroblasts
indicating that it may be a compensatory response to inflammation. Preventing this response by genetic deletion of *ITPR2*
from SOD1^{G93A} mice had a dose-dependent effect on disease duration, resulting in a significantly shorter lifespan of these
mice. In addition, the absence of *IP$_3$R2* led to increased innate immunity, which may contribute to the decreased survival of
the SOD1^{G93A} mice. Besides systemic inflammation, *IP$_3$R2* knockout mice also had increased IFNγ, IL-6 and IL1α expression.
Altogether, our data indicate that *IP$_3$R2* protects against the negative effects of inflammation, suggesting that the increase
in *IP$_3$R2* expression in ALS patients is a protective response.

Introduction

Amyotrophic lateral sclerosis (ALS) is a devastating neurodegenerative disease caused by the progressive loss of motor neurons and denervation of muscle fibres, resulting in muscle weakness and paralysis. The disease has an incidence of 2.7 per 100,000 people in Europe (1). In the absence of a medical cure, average life expectancy post-diagnosis is between 2 and 5 years. On average, 10% of ALS cases are familial, of which 20% are caused by mutations in superoxide dismutase 1 (*SOD1*) on the basis of which ALS mouse models have been developed. As disease progression is indistinguishable between familial and sporadic ALS, common disease mechanisms are expected. ALS pathophysiology is non-cell autonomous (2), and increased expression of several cytokines is detected in both patients (3) and rodent models of the disease (4). Increasing inflammation in ALS model mice is detrimental to survival (5,6), although inflammation is not hypothesized to be a primary cause of human ALS (7).

Genome-wide association analysis linked the inositol 1,4,5-trisphosphate receptor 2 gene (*ITPR2*) to ALS and increased *ITPR2* gene expression was found in blood samples of sporadic ALS patients (8). This genetic association was not replicated in other studies (9,10). Although recent exome sequencing of case-unaffected–parents trios identified a *de novo* variant in *ITPR2* (11), the potential role of this variant remains unclear. The higher *ITPR2* gene expression in ALS also remains intriguing due to the important role of the gene product of *ITPR2*, the inositol 1,4,5-trisphosphate receptor 2 (IP_3R2), in calcium signalling. IP$_3$Rs release calcium from the endoplasmic reticulum (ER) into the cytosol after binding of IP$_3$ (12). IP_3R2 has a high amino acid conservation (13,14) and is expressed by different cell types, including astrocytes (15–17), oligodendrocytes (18), Schwann cells (19), macrophages, neutrophils and mast cells (20). It is also the most sensitive isoform of the IP$_3$ receptors essential for ER calcium release in astrocytes (21), affecting the plasticity or the baseline synaptic activity of hippocampal neurons (21–23). IP_3R2 knockout mice do not have a distinct phenotype (24).

Calcium signalling plays an important role in motor neurons and could explain the selective vulnerability of motor neurons as well as the therapeutic effect of the only registered drug for ALS (riluzole) (25). By decreasing glutamate release, riluzole diminishes excitotoxicity, which is at least partially due to an increase in intracellular calcium. Apart from calcium influx due to the relatively high level of Ca^{2+}-permeable AMPA receptors on motor neurons (26), we previously showed that higher calcium release from intracellular stores by overexpression IP_3R2 in neurons has a negative effect on the disease process in ALS mice (27). On the other hand, genetic removal of an enzyme responsible for IP$_3$ formation, phospholipase C delta, prolongs survival of SOD1^{G93A} mice (28). Moreover, the calcium release systems in the ER play a crucial role in the ER-mitochondria calcium cycle of which a disturbance could lead to the increased ER stress response observed in ALS (29,30).

To investigate the relevance of increased *ITPR2* expression in ALS patients, we studied the expression of *ITPR2* in SOD1^{G93A} mice and in several other models of both chronic and acute neurodegeneration, as well as after induction of systemic inflammation. To evaluate the functional relevance of the observed increase in *ITPR2* expression, we genetically removed one or both *ITPR2* alleles from SOD1^{G93A} mice and determined its effect on disease onset and survival. In addition, we characterized IP_3R2 knockout mice and discovered disturbances in innate immunity, as well as increased IFNγ and IL1α expression

levels. Our data indicate that IP_3R2 has a novel anti-inflammatory function that may modify the ALS disease progression.

Results

IP$_3$R2 expression is increased in neurodegenerative disease models and after LPS stimulation

To investigate the role of *ITPR2* in ALS, we assessed whether *ITPR2* gene expression was increased in a mouse model of ALS. We performed quantitative PCR (qPCR) on ventral spinal cords of control and SOD1^{G93A} mice at different disease stages. A significant upregulation of *ITPR2* gene expression was detected in the ventral spinal cords of symptomatic and end stage SOD1^{G93A} mice compared to non-transgenic and SOD1^{WT} mice (Fig. 1A). This upregulation in the spinal cord of ALS mice was specific to IP_3R2, as the other IP$_3$R isoforms (IP_3R1 and IP_3R3) did not increase during disease (Supplementary Material, Fig. S1A–B). We were unable to confirm these differences at the protein level due to the lack of specific IP_3R2 antibodies without cross reactivity to IP_3R1 and/or IP_3R3 on Western blot or immunohistochemistry.

To investigate whether the upregulation of *ITPR2* expression is unique for ALS, we determined IP_3R2 gene expression in other models of neurodegeneration, both chronic and acute and affecting either the spinal cord or brain. In a murine model of multiple sclerosis, experimental autoimmune encephalomyelitis (EAE) characterized by pronounced inflammation at lesion sites, increased IP_3R2 gene expression was also detected by qPCR in the lumbar spinal cord of affected mice (Fig. 1B). This was also observed in an acute model of neurodegeneration, as increased IP_3R2 gene expression was detected in the penumbra of photothrombotic cortical stroke (Fig. 1C). To analyse whether the upregulation of the IP$_3$R in the above conditions was specific to type 2 of the receptor, qPCR analysis of IP_3R1 and IP_3R3 was performed on the same tissues. There was no upregulation of IP_3R1 or IP_3R3 in EAE affected lumbar spinal cords (Supplementary Material, Fig. S2A–B) or in stroke penumbra (Supplementary Material, Fig. S2C–D), indicating that the upregulation is indeed IP$_3$R isoform 2 specific.

To assess whether induction of inflammation also modulates IP_3R2 gene expression, we treated different cell types *in vitro* with lipopolysaccharide (LPS). Murine primary astrocytes and murine peritoneal macrophages dose-dependently increased IP_3R2 expression when treated with LPS (Fig. 1D and E). This effect seems also specific to IP_3R2, as gene expression of IP_3R1 and IP_3R3 was not significantly increased by LPS in murine astrocytes (Supplementary Material, Fig. S2E and F). Altogether, these data indicate that IP_3R2 may play a role in inflammation.

Genetic ablation of *IP$_3$R2* is detrimental in SOD1^{G93A} mice

To investigate the functional relevance of the *ITPR2* upregulation in ALS, we crossbred IP_3R2 knockout ($IP_3R2^{-/-}$) mice with SOD1^{G93A} mice. We first analysed by qPCR the IP_3R2 expression in the ventral spinal cord of $IP_3R2^{-/-}$ mice. As expected, IP_3R2 gene expression was ablated in $IP_3R2^{-/-}$ mouse and was reduced by 50% in the $IP_3R2^{+/-}$ ventral spinal cord (Fig. 2B). There was no compensation by increased mRNA expression of IP_3R1 (Fig. 2A) or IP_3R3 (Fig. 2C).

The genetic ablation of IP_3R2 in SOD1^{G93A} did not affect significantly the age of disease onset between genotypes as
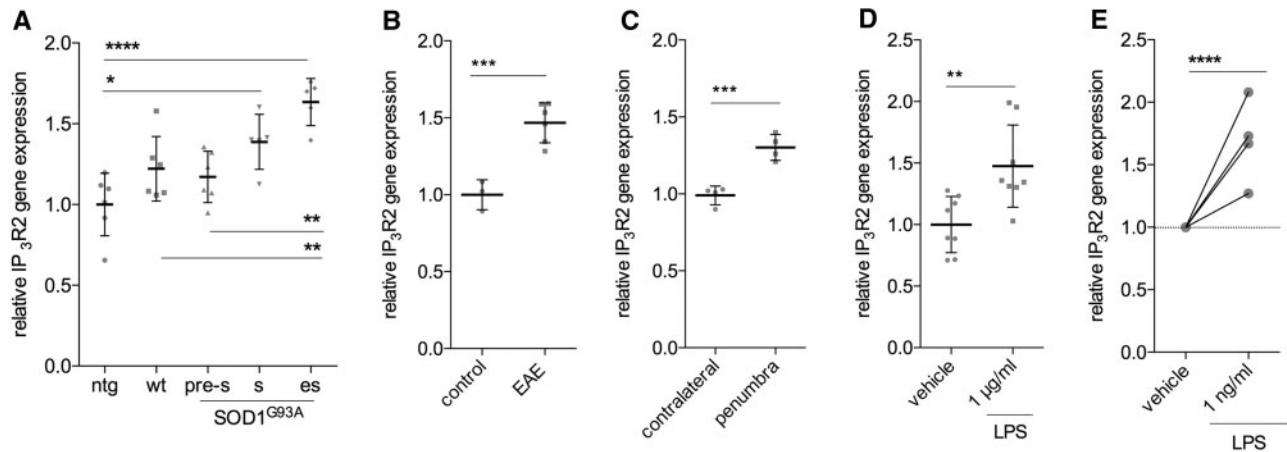
Figure 1. Relative IP_3R2 gene expression is increased in models of neurodegeneration and inflammation. (**A**) Relative gene expression of IP_3R2 assessed by qPCR on ventral spinal cords of non-transgenic (ntg; $n = 6$), $SOD1^{WT}$ (wt; $n = 6$), pre-symptomatic $SOD1^{G93A}$ (pre-s; $n = 6$), symptomatic $SOD1^{G93A}$ (s; $n = 5$) and end stage $SOD1^{G93A}$ (es; $n = 5$) mice (ANOVA, Bonferroni post-hoc). (**B**) Relative IP_3R2 gene expression analysed in the lumbar spinal cord of severely affected EAE-mice ($n = 3$) and control mice ($n = 6$) by qPCR (unpaired t-test). (**C**) Relative IP_3R2 gene expression analysed in the penumbra zone of stroke in mice ($n = 4$) and a similar region in the contralateral side of the brain by qPCR (paired t-test). (**D**) Relative IP_3R2 gene expression in ventral spinal cord astrocytes *in vitro* by 24 h LPS application ($n = 8$) or vehicle ($n = 8$; unpaired t-test). (**E**) Relative IP_3R2 gene expression in murine macrophages ($n = 4$; Wilcoxon signed rank test compared to 1.0, two-tailed). The dotted line reflects the normalising vehicle condition set at 1. Mean $\pm$ standard deviation. $^*P < 0.05$, $^{**}P < 0.01$, $^{***}P < 0.001$, $^{****}P < 0.0001$.

assessed by the hanging wire test (Fig. 2D), nor by the rotarod (Fig. 2E). Remarkably, there was a considerable and dose-dependent effect on the survival of ALS mice (Fig. 2F). This dose-dependency was consistent with the 50% expression of IP_3R2 in $IP_3R2^{+/-}$ ventral spinal cords compared to $IP_3R2^{+/+}$ mice (Fig. 2B). The detrimental effect of IP_3R2 knockdown on disease progression was also shown in the decreased levels of relative grip strength between genotypes for the fore paws (Fig. 2G) and all paws (Fig. 2H). The number of motor neurons in the ventral horn of the lumbar spinal cord is lower in $IP_3R2^{-/-}$ $SOD1^{G93A}$ mice than in $IP_3R2^{+/+}$ $SOD1^{G93A}$ mice at 145 days of age (Fig. 2I), as expected due to increased disease severity in $IP_3R2^{-/-}$ $SOD1^{G93A}$ mice at this age. The difference in survival is not likely due to a higher intrinsic vulnerability of $IP_3R2^{-/-}$ neurons, as their basal survival *in vitro* is not different compared to non-transgenic motor neurons (Fig. 2J). In addition, astrogliosis and microgliosis of the ventral horn of the lumbar spinal cord of $IP_3R2^{+/+}$ $SOD1^{G93A}$ and $IP_3R2^{-/-}$ $SOD1^{G93A}$ mice seemed comparable at the end stage (Supplementary Material, Fig. S3). Altogether, our data show that genetic ablation of IP_3R2 is detrimental for motor neuron survival in $SOD1^{G93A}$ mice.

IP_3R2 knockout mice have increased inflammatory potential

In view of the effect of inflammation on IP_3R2 expression (Fig. 1) and to understand the mechanism responsible for the more rapid disease progression in $IP_3R2^{-/-}$ $SOD1^{G93A}$ mice, we investigated the relative contribution of immune cells in adult $IP_3R2^{+/+}$ and $IP_3R2^{-/-}$ mice by flow cytometry. Within the adaptive immune system, there was no difference in the relative number or activation status of B cells or T cells (Supplementary Material, Fig. S4A–D). By contrast, large changes were observed in the myeloid populations. The relative number of Ly6C^{hi} monocytes was increased in both the spleen and blood of $IP_3R2^{-/-}$ mice (Fig. 3A and B). This effect was also observed with LyC6^{lo} monocytes in $IP_3R2^{-/-}$ mice, in both the spleen and blood (Fig. 3C and D). Neutrophils and dendritic cells were present in normal proportions (Supplementary Material, Fig.

S5). These data imply that there is an increased potential for systemic innate inflammation in the $IP_3R2^{-/-}$ mouse.

To study the presence of systemic inflammation, we assessed interferon gamma (IFNγ) and interleukin 6 (IL6) in the serum of adult $IP_3R2^{+/+}$ and $IP_3R2^{-/-}$ mice. IFNγ levels were increased in the serum of unchallenged $IP_3R2^{-/-}$ mice (Fig. 3E) and a similar trend was observed for IL6 (Fig. 3F). A (dose-dependent) role for IL-6 in the ventral spinal cord of $IP_3R2^{+/+}$, $IP_3R2^{+/-}$ and $IP_3R2^{-/-}$ mice is detected by qPCR analysis (Fig. 3G). To determine the potential role of IP_3R2 in induced neuroinflammation, we assessed the expression of the pro-inflammatory cytokine IL1α *in vitro* in embryonic ventral spinal cord astrocytes when treated with LPS. Here, we detected an increase of IL1α with decreasing copies of IP_3R2 (Fig. 3H). This is in accordance with our observations *in vivo* upon photothrombotic stroke, where the penumbra and stroke zone of $IP_3R2^{-/-}$ mice has increased gene expression of $IL1α$ (Fig. 3I). Together, these data imply that genetic ablation of IP_3R2 causes increased propensity to inflammation, which may infer an exacerbated disease progression in $SOD1^{G93A}$ mice (Fig. 2F).

Discussion

In this study, we show that the *ITPR2* gene expression is significantly upregulated in ALS and in other models of neurodegeneration, as well as after induction of inflammation. This upregulation of *ITPR2* expression may be a compensatory protective response in ALS, as genetic deletion of IP_3R2 exacerbates ALS disease progression in $SOD1^{G93A}$ mice and decreases survival dose-dependently. At first sight, this negative effect of IP_3R2 deletion is contra intuitive as it results in motor neurons in a lower intracellular calcium concentration in response to IP_3-inducing agents. This could theoretically result in a higher resistance to excitotoxic damage as we have shown before that expression of more IP_3R2 in neurons has a negative effect (27), while genetic ablation of an enzyme involved in the production of IP_3 has a beneficial effect on the survival of $SOD1^{G93A}$ mice (28). In addition, a lower number of IP_3Rs in the ER could
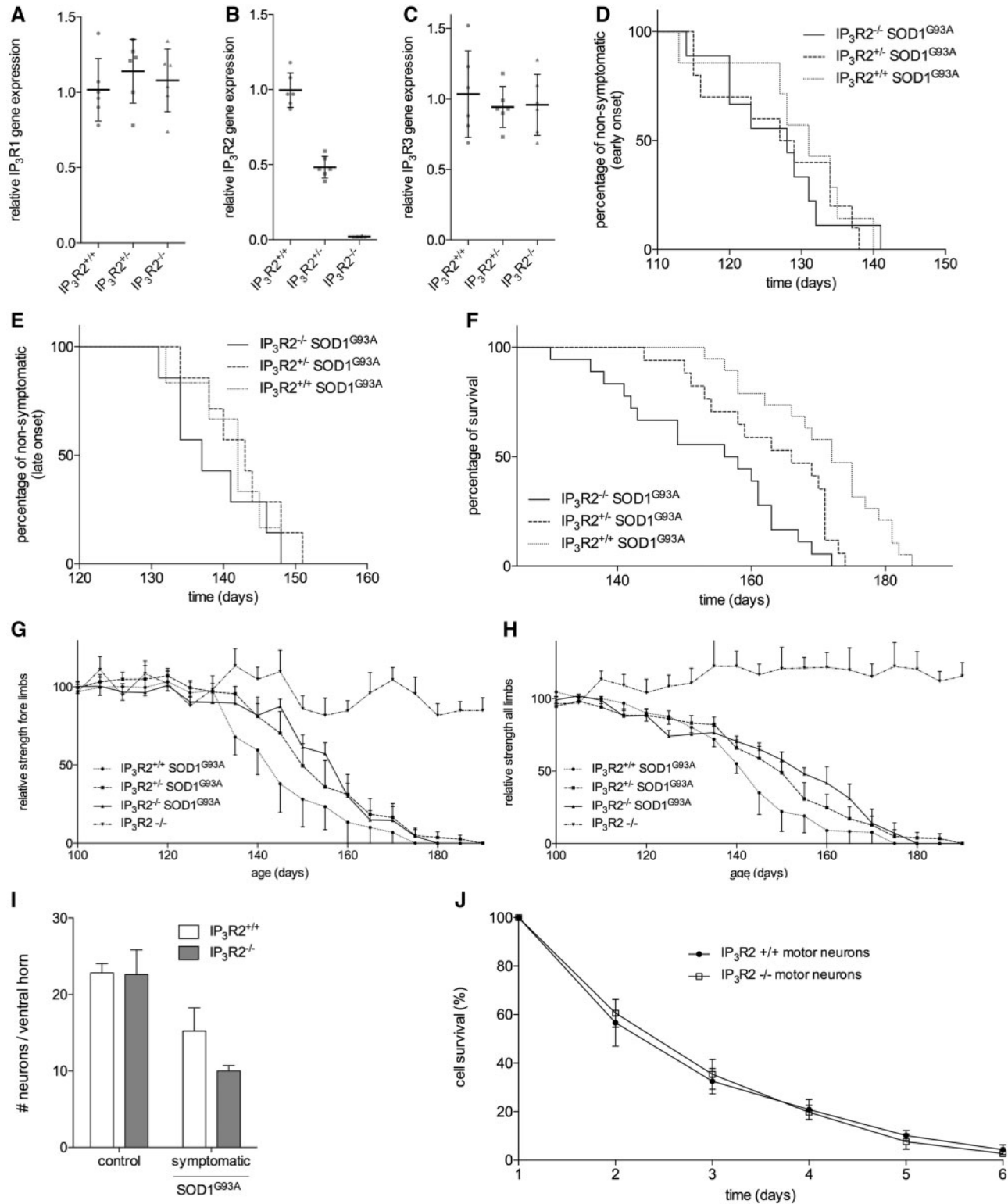
Figure 2. IP$_3$R2 knockout exacerbates disease in SOD1^{G93A} mice. Relative gene expression of IP$_3$R1 (**A**), IP$_3$R2 (**B**) and IP$_3$R3 (**C**) assessed by qPCR in ventral spinal cords of IP$_3$R2$^{+/+}$ ($n=6$), IP$_3$R2$^{+/-}$ ($n=6$) and IP$_3$R2$^{-/-}$ ($n=6$) mice. (**D**) Early symptom onset as determined by the hanging wire test between IP$_3$R2$^{+/+}$ SOD1^{G93A} ($n=6$; 129.7 ± 8.6 days), IP$_3$R2$^{+/-}$ SOD1^{G93A} ($n=7$; 126.8 ± 9.1 days) and IP$_3$R2$^{-/-}$ SOD1^{G93A} mice ($n=7$; 126.4 ± 8.1 days, Log-rank, $P=0.88$). (**E**) Late symptom onset as determined by the rotarod test between IP$_3$R2$^{+/+}$ SOD1^{G93A} ($n=6$; 141.2 ± 5.1 days), IP$_3$R2$^{+/-}$ SOD1^{G93A} ($n=7$; 142.6 ± 5.4 days) and IP$_3$R2$^{-/-}$ SOD1^{G93A} mice ($n=7$; 138.7 ± 6.0 days, Log-rank, $P=0.55$). (**F**) Survival analysis by determining the age of end stage of IP$_3$R2$^{+/+}$ SOD1^{G93A} ($n=19$; 170.7 ± 9.6 days), IP$_3$R2$^{+/-}$ SOD1^{G93A} ($n=17$; 162.8 ± 9.6 days) and IP$_3$R2$^{-/-}$ SOD1^{G93A} ($n=18$; 153.2 ± 12.5 days; Log-rank, $P<0.0001$). (**G-H**) Disease progression as measured by grip strength of IP$_3$R2$^{+/+}$ SOD1^{G93A} mice ($n=5$), IP$_3$R2$^{+/-}$ SOD1^{G93A} mice ($n=7$), IP$_3$R2$^{-/-}$ SOD1^{G93A} mice ($n=6$) and IP$_3$R2$^{-/-}$ mice ($n=4$) for the fore limbs (G) and all limbs (H). (**I**) Quantification of neurons from lumbar spinal cord in adult IP$_3$R2$^{+/+}$ ($n=3$) IP$_3$R2$^{-/-}$ ($n=3$) and 145 day old IP$_3$R2$^{+/+}$ SOD1^{G93A} ($n=3$) and IP$_3$R2$^{-/-}$ SOD1^{G93A} mice ($n=2$; 2-way ANOVA disease stage $P=0.0061$). (**J**) The viability of murine motor neurons isolated from IP$_3$R2$^{-/-}$ ($n=4$) and non-transgenic ($n=4$) plated on non-transgenic rat astrocytic feeder layers in serum-enriched media. Mean ± standard deviation.
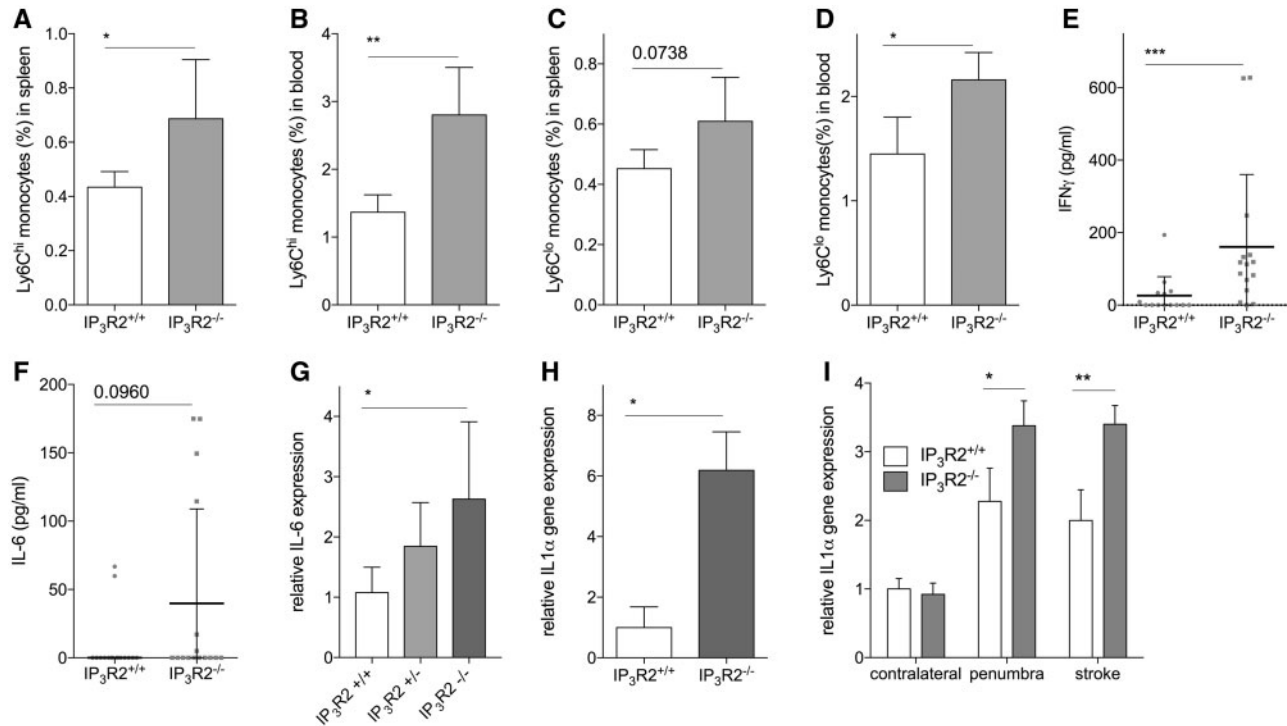
Figure 3. Relative amounts of Ly6C^{hi} and Ly6C^{lo} monocytes as determined by FACS in adult *IP$_3$R2$^{+/+}$* and *IP$_3$R2$^{-/-}$* mice. (**A**) Relative amount of Ly6C^{hi} monocytes in the spleen of *IP$_3$R2$^{+/+}$* ($n = 7$) and *IP$_3$R2$^{-/-}$* mice ($n = 8$; unpaired *t*-test). (**B**) Relative amount of of Ly6C^{hi} monocytes in blood of *IP$_3$R2$^{+/+}$* ($n = 7$) and *IP$_3$R2$^{-/-}$* mice ($n = 8$; unpaired *t*-test). (**C**) Relative amount of Ly6C^{lo} monocytes in spleen of *IP$_3$R2$^{+/+}$* ($n = 6$) and *IP$_3$R2$^{-/-}$* mice ($n = 8$; unpaired *t*-test). (**D**) Relative amount of Ly6C^{lo} monocytes in blood of *IP$_3$R2$^{+/+}$* ($n = 6$) and *IP$_3$R2$^{-/-}$* mice ($n = 8$; unpaired *t*-test). (**E**) Level of IFNγ in the serum of *IP3R2$^{+/+}$* mice ($n = 14$) and *IP3R2-/-* mice ($n = 14$; Mann-Whitney). (**F**) Level of IL-6 in the serum of *IP$_3$R2$^{+/+}$* mice ($n = 14$) and *IP$_3$R2$^{-/-}$* mice ($n = 14$; Mann-Whitney). (**G**) Relative IL-6 gene expression assessed by qPCR in ventral spinal cords of *IP$_3$R2$^{+/+}$* ($n = 6$), *IP$_3$R2$^{+/-}$* ($n = 5$) and *IP$_3$R2$^{-/-}$* mice (ANOVA, Bonferroni correction for multiple testing). (**H**) Relative IL1α gene expression of embryonic ventral spinal cord astrocytes from *IP$_3$R2$^{+/+}$* ($n = 2$) and *IP$_3$R2$^{-/-}$* ($n = 2$) mice treated with LPS (unpaired *t*-test). (**I**) Relative IL1α gene expression of the stroke zone, penumbra and contralateral side 7 days after photothrombotic stroke in *IP$_3$R2$^{+/+}$* ($n = 5$) and *IP$_3$R2$^{-/-}$* mice ($n = 3$; 3 unpaired *t*-tests). Mean ± standard deviation. * $P < 0.05$, ** $P < 0.01$, *** $P < 0.001$.

counteract the calcium depletion of this organelle. This will have a positive effect on the ER stress and protein misfolding that are the consequences of disturbances in the ER-mitochondria calcium cycle observed in motor neurons (29,30). However, IP$_3$R2 is not only expressed in (motor) neurons. On the contrary, IP$_3$R2 is an important isoform in a number of non-neuronal cells (15–20). As a consequence, the potential beneficial effect of removing IP$_3$R2 in motor neurons seems to be outnumbered by the negative effect of IP$_3$R2 removal in the other cell types.

As a consequence, we hypothesize that the negative effect of IP$_3$R2 expression on motor neurons is due to the loss of anti-inflammatory function exerted by IP$_3$R2 when it is genetically ablated from all cell types. That inflammation harbours a negative effect on survival of ALS mice has been shown previously by increasing inflammation by LPS injections (6) and M-CSF administration (5). The role of IP$_3$R2 in this process is new and unexpected. However, inflammation is also observed in IP$_3$R2 and IP$_3$R3 double knockouts in olfactory endothelium and lacrimal glands as increased levels of TNFα, MIP-2 and IL-6 gene expression are detected (31). These double knockouts show defects in the function of secretory epithelial cells (24,31), while IP$_3$R1 and IP$_3$R2 double knockout results in perturbations of cardiogenesis causing embryonic death (32). For a long time, it was supposed that genetic ablation of solely IP$_3$R2 has no effect. Recently, a reduction in sweat production was reported (33). Our data indicate that the inflammatory potential is also affected.

These data are in line with the hypothesis that the upregulation of IP$_3$R2 during inflammation is an inherent mechanism of

the cell to reduce production of pro-inflammatory cytokines, by increasing intracellular calcium to block MAPK activation. IP$_3$R2 is particularly useful in this context as it is the most sensitive receptor subtype to IP$_3$. Our study demonstrates that upregulation of ITPR2 occurs in primary murine astrocytes and murine macrophages upon inflammation. Although an increase in ITPR2 gene expression *in vivo* may be explained by infiltrating cell types rich in ITPR2 expression, *in vitro* work with non-proliferating astrocytes in culture demonstrates that ITPR2 expression can be increased per cell post-stimulation. Furthermore, ITPR2 upregulation is also observed in HUVEC and epithelial cells after stimulation with anti-inflammatory treatment with Serp-1, which may explain in part the anti-inflammatory mechanism of Serp-1 (34).

One possible pathway in which IP$_3$R2 could play a role in inflammation is linked to the stimulation of metabotropic glutamate receptors (mGluRs). This activates phospholipase C (PLC) to hydrolyse phosphatidylinositol 4,5-bisphosphate (PIP$_2$) into diacylglycerol (DAG) and IP$_3$. The latter activates IP$_3$ receptors that allow ER calcium release. This higher cytoplasmic calcium concentration could block the activation of MAPK and cytokine/chemokine transcription. Interestingly, there are multiple mGluRs expressed by glia and activation of some of these may be anti-inflammatory. A role of mGluRs in neuroinflammation has been shown in cultured microglia in which activation of mGluR5 inhibits inflammation and neurotoxicity (35). An upregulation of mGluRs is found on astrocytes in both ALS (36,37) and MS patients (38) and is correlated to glial fibrillary acidic protein (GFAP) expression (36). It was also shown that an

increase in IP$_3$ formation and intracellular calcium concentration occurs in reactive cells, including astrocytes, in culture (39–42) and this is inhibited by blocking PLC (40). Genetically ablating *IP$_3$R2* could result in a disinhibition of MAPK activation that increases cytokine/chemokine transcription, as intracellular calcium blocks MAPK activation (42,43). Furthermore, pharmacological approaches have shown that inhibition of PLC or IP$_3$ receptors or intracellular calcium chelation with BAPTA-AM increase the production of cytokines/chemokines in a variety of cell types including microglia (35,44), oligodendrocytes (45), hematopoietic stem cells/progenitor cells (42), monocytes/alveolar macrophages (46), neutrophils (47) and vascular smooth muscle cells (48). Interestingly, this process has not yet been associated with *IP$_3$R2*.

In conclusion, we report a novel role of *ITPR2* in inflammation and a detrimental effect of genetic ablation of *ITPR2* in ALS. Altogether, our data suggest that this anti-inflammatory function of *ITPR2* may be effectively targetable in a number of cell types and (inflammatory) disorders, including ALS.

Materials and Methods

Animal studies

IP$_3$R2 knockout mice, described previously (24), were intercrossed with high-copy number *SOD1^{G93A}* (The Jackson Laboratory, Bar Harbor, USA). Human wild-type SOD1 overexpressing mice (*SOD1^{WT}*) were obtained from The Jackson Laboratory for use as controls. All mice were on a C57BL/6 background. *IP$_3$R2* knockout mice, *SOD1^{G93A}* mice and *SOD1^{WT}* mice were housed in standard conditions in the conventional housing facility of the University of Leuven with food and water *ad libitum*. Experiments performed at the University of Leuven were performed according to the guidelines of the University of Leuven and have received ethical committee approval (project codes 143/2008, 150/2009, 158/2009, 020/2010, 085/2011). Experiments performed at the Vrije Universiteit Brussel, were approved by the Ethical Committee for Animal Experiments (ECAE) at the Vrije Universiteit Brussel (project number 11-220-13), and all animal experiments met the standards required by the Belgian Council for Laboratory Animal Science (BCLAS) guidelines.

Motor testing and determination of survival

The hanging wire test was used to determine early disease onset by assessing the ability of the mice to hold their own weight for 60 s, as previously described (49). Briefly, we placed a mouse on a wire grid and turned it over while the mouse was holding its own body weight upside-down. If a mouse failed (dropped from the grid before 60 s) and in consecutive trials could not hold its own weight for 60 s, it was defined as symptomatic. The rotarod (Ugo Basile, Varese, Italy) is used to determine late stage disease onset. After training and consistent baseline measurements (5 measurements of maximal scores of 300 s on different days), mice are provided with three trials of 300 s. The average of the 3 trials per mouse is calculated (the length of time they remain on the rod) and symptom onset is defined as the first measurement when the average is less than 60 s and never increases above again. Grip strength measurements were performed with a dynamometer (Chatillon, Largo, FL, USA) every 5 days from 80 days of age onwards at which grip strength was determined with the mice holding a bar (fore limbs only) or when placed on a small grid (all limbs). Relative grip strength

was determined per mouse by normalising the absolute grip strength (N) values to the average for each mouse from day 90 to day 105. End stage was determined when mice were unable to rear themselves within 30 s when placed on their back (also described as survival). Extra attention was paid to assess mice in comparison to their littermate controls.

Chronic progressive, experimental autoimmune encephalomyelitis

Experimental autoimmune encephalomyelitis (EAE) was induced by injecting C57BL/6 mice subcutaneously with 100 μg MOG peptide (Eurogentec, Fremont, CA, USA) and 400 μg mycobacterium butyricum (Difco, Becton Dickinson, Franklin Lakes, USA) in complete Freund's adjuvant (CFA) at three sites in the back. Mice received 400 ng Bordetella pertussis toxin (Calbiochem, Darmstadt, Germany) in NaCl 0.9% intraperitoneally (IP) at the time of immunization and 48 h later to disrupt the blood-brain barrier and lumbar spinal cord tissue was collected at 18 weeks.

Photothrombotic cortical stroke

Focal cortical ischemia was induced in female C57BL/6J mice aged at least 3 months by photothrombosis, as previously described (50). Mice were anesthetized with 2.5% isoflurane (Halocarbon, New Jersey, USA) in an oxygen/air mixture and rectal temperature during the surgical procedure was maintained at $37 \pm 0.5\,°C$ with a heating plate (TCAT-2LV Controller, Physitemp instruments, New Jersey, USA). After fixation in a stereotactic frame (David Kopf Instruments, Bilaney, Germany) the skull was exposed by a midline incision in the skin. Rose Bengal (Sigma, ST. Louis, MO, USA), 0.1 ml with a concentration of 3 mg/ml in normal saline, was infused by tail vein injection. For illumination, a laser beam of wavelength 565 nm (L4887-13, Hamamatsu Photonics, Japan) with a aperture of 1.8 mm was focused 0.5 mm anterior and 1.8 mm right of the bregma. The brain was illuminated immediately after Rose Bengal injection during 5 min through the intact skull. Seven days after stroke mice were perfused with PBS and the brain was dissected for mRNA extraction of the following regions: stroke zone, peri-infarct area, ipsilateral and contralateral cortex.

Quantitative PCR analysis

Isolation of mRNA from ventral spinal cord occurred by the TriPure (Roche, Basel, Switzerland) method and reverse transcriptase PCR with random hexamers (Life Technologies, Carlsbad, USA) and M-MLV (Invitrogen, Life Technologies). Quantitative Real-Time PCR (qPCR) analysis was performed with the StepOnePlus (Life Technologies) with TaqMan Universal PCR Master Mix (Life Technologies). All murine analyses were confirmed by at least two housekeeping genes. Assays were purchased from Life Technologies and IDT DNA and the signal quantified with the ΔΔCT method.

Protein levels determination

Serum was collected from mice directly after euthanization and approx. 100 μl shipped frozen to Aushon Biosystems (Billerica, MA, USA) for multiplexed SearchLight immunoassays. Data were analysed by an investigator blinded to the genotypes of the samples tested.

(Motor) neuron quantification

To visualize neurons, Nissl staining was performed on 4% formaldehyde-fixed spinal cord sections. Sections were briefly immersed in a cresyl violet solution and subsequently in a 70% ethanol with 10% acetic acid. Slides were dehydrated by an increased ethanol concentration series and mounted with PerTex® (Histolab AB, Goteborg, Sweden). Images were collected by Zeiss Axio Imager M1 microscope (Carl Zeiss AG, Jena, Germany) with AxioCam Mrc5 camera (Carl Zeiss AG). The number of (motor) neurons was quantified by measurement of the soma area as visualized by cresyl violet staining in ImageJ (National Institute for Health) on multiple 40 μm thick sections in the ventral horn of the lumbar spinal cord. Characterization of motor neurons occurred as previously (51) on at least five ventral horns of the lumbar spinal cord of 2–3 mice per group.

Immunohistochemistry

Mice were transcardially perfused with phosphate buffered saline (PBS) and subsequently with 4% formaldehyde. Spinal cords were post-fixed with 4% formaldehyde overnight at 4 °C and transferred to 30% sucrose for an additional night. After snap freezing, tissue was sectioned by cryostat at 40 μm thickness and stained with antibodies against glial fibrillary acidic protein (GFAP, Santa Cruz Biotechnology, Santa Cruz, USA) and Iba1 (Wako, Japan). Secondary antibodies for immunofluorescence include Alexa-555 and Alexa-488 (Invitrogen). Vectashield with DAPI (Vector, Burlingame, CA) was used for mounting spinal cord sections. Images were collected by Zeiss Axio Imager M1 microscope (Carl Zeiss AG) with AxioCam Mrc5 camera (Carl Zeiss AG).

LPS treatment *in vitro*

Primary cultures of neurons and astrocytic feeder layers were isolated on E13.5 as previously described (26). Astrocytes from each embryo were divided over two wells on a 12-well plate and were allowed to grow until each well was fully covered. They were subsequently treated with arabinofuranosyl cytidine (VWR International, Leuven, Belgium) for at least 24 h to halt proliferation of the astrocytes and remove any other cell types present. Thereafter the medium was replaced for 24 h with media without penicillin and streptomycin (Invitrogen), collected and replaced with penicillin and streptomycin free media containing either 1 μg/ml of LPS or vehicle (H$_2$O). Cells were lysed and mRNA preserved. The mRNA extraction occurred by the TriPure method and was purified with the RNeasy Qiagen kit according to the manufacturer's guidelines.

Thioglycolate-elicited peritoneal macrophages (thio-PEM) were obtained from non-transgenic C57BL/6-mice by IP injection of 3 ml thioglycolate (bioMérieux, Marcy l'Etoile France). At day 4, mice were killed, followed by a peritoneal lavage with 10 ml PBS/10% sucrose. Extracted cells were counted and seeded in 6-well culture plates (Falcon, Becton Dickinson) at a concentration of 5 × 10^6 cells/well. After 3 h incubation at 37° C and 5% CO$_2$, non-adherent cells were washed away with PBS and plastic-adherent peritoneal macrophages were used for analysis. Thio-PEM were subjected to stimulation by 1 ng/ml or 100 ng/ml bacterial LPS (055:B5, Sigma). After 24 h of incubation at 37 °C and 5% CO$_2$, RNA was extracted from each condition by TRIzol® Reagent (Invitrogen), and cDNA was synthesized. This cDNA was then used for quantitative PCR. Correct stimulation of the macrophages was confirmed by verifying the gene expression profile of inducible nitric oxide synthase (iNOS).

Fluorescent cytometry analysis

Single-cell suspensions were prepared from spleen and blood. Erythrocytes were depleted by lysis with NH$_4$Cl$_2$ solution. Peritoneal fluid was collected after lavage with cold and sterile PBS. Murine cells were harvested and cultured in Roswell Park Memorial Institute (RPMI) media with 10% foetal calf serum (FCS) plus supplement (glutamine, 2-mercaptoethanol, penicillin and streptomycin, and 10 mM HEPES). For cell-surface staining, 2–3 × 10^6 cells per sample were incubated with various antibodies in staining buffer (PBS and 3% FCS) for 20 min at 4 °C. After 4 h of incubation in media with PMA (50 ng/ml) and ionomycin (500 ng/ml) intracellular cytokine staining was performed according to the manufacturer's guidelines for the BD Biosciences-Pharmingen Fixation/Permeabilization Solution Kit. Anti-murine antibodies included B220 (RA3-6B2), CD4 (GK1.5), CD8 (53-6.7), CD69 (H1.2F3), CD62L (MEL-14), CD44 (IM7), Gr-1 (RB6-8C5), CD11b (M1/70), CD11c (N418), F4/80 (BM8), Ly6C (HK1.4), MHCII (M5/114.15.2) and IFNγ (XMG1.2) all from eBioscience (San Diego, USA). Data were acquired on a Canto I flow cytometer (BD Biosciences, New Jersey, USA) and analysed using FlowJo for Mac version 9.2 (Tree Star Inc., Ashland, USA).

Statistical analysis

Analysis was performed with the statistical software package Prism Origin. Survival and disease onset was analysed by Log-Rank. Multiple group analyses were performed by ANOVA followed by Bonferroni post hoc analysis. Differences over 2 groups were analysed by Student's *t*-test and the Mann-Whitney test or Wilcoxon signed rank test, as described, when a non-normal distribution of the data is assumed. Significance was assumed at $P < 0.05$. Graphs represent the mean ± standard deviation.

Supplementary Material

Supplementary Material is available at *HMG* online.

Acknowledgements

Funding

References

1. Logroscino, G., Traynor, B.J., Hardiman, O., Chio, A., Mitchell, D., Swingler, R.J., Millul, A., Benn, E. and Beghi, E. and EURALS(2009) Incidence of amyotrophic lateral sclerosis in Europe. *J. Neurol. Neurosurg. Psychiat.*, **81**, 385–390.

2. Ilieva, H., Polymenidou, M. and Cleveland, D.W. (2009) Non-cell autonomous toxicity in neurodegenerative disorders: ALS and beyond. *J. Cell Biol.*, **187**, 761–772.

3. Aebischer, J., Moumen, A., Sazdovitch, V., Seilhean, D., Meininger, V. and Raoul, C. (2012) Elevated levels of IFNgamma and LIGHT in the spinal cord of patients with sporadic amyotrophic lateral sclerosis. *Eur. J. Neurol.*, **19**, 752–759.

4. Beers, D.R., Zhao, W., Liao, B., Kano, O., Wang, J., Huang, A., Appel, S.H. and Henkel, J.S. (2011) Neuroinflammation modulates distinct regional and temporal clinical responses in ALS mice. *Brain Behav. Immun.*, **25**, 1025–1035.

5. Gowing, G., Lalancette-Hebert, M., Audet, J.N., Dequen, F. and Julien, J.P. (2009) Macrophage colony stimulating factor (M-CSF) exacerbates ALS disease in a mouse model through altered responses of microglia expressing mutant superoxide dismutase. *Exp. Neurol.*, **220**, 267–275.

6. Nguyen, M.D., D'Aigle, T., Gowing, G., Julien, J.P. and Rivest, S. (2004) Exacerbation of motor neuron disease by chronic stimulation of innate immunity in a mouse model of amyotrophic lateral sclerosis. *J. Neurosci.*, **24**, 1340–1349.

7. Poppe, L., Rue, L., Robberecht, W. and Van Den Bosch, L. (2014) Translating biological findings into new treatment strategies for amyotrophic lateral sclerosis (ALS). *Exp. Neurol.*, **262**, 138–151.

8. van Es, M.A., Van Vught, P.W., Blauw, H.M., Franke, L., Saris, C.G., Andersen, P.M., Van Den Bosch, L., de Jong, S.W., van 't Slot, R., Birve, A., *et al.* (2007) ITPR2 as a susceptibility gene in sporadic amyotrophic lateral sclerosis: a genome-wide association study. *Lancet Neurol.*, **6**, 869–877.

9. Fernandez-Santiago, R., Sharma, M., Berg, D., Illig, T., Anneser, J., Meyer, T., Ludolph, A. and Gasser, T. (2011) No evidence of association of FLJ10986 and ITPR2 with ALS in a large German cohort. *Neurobiol. Aging*, **32**, 551 e551–554.

10. Chio, A., Schymick, J.C., Restagno, G., Scholz, S.W., Lombardo, F., Lai, S.L., Mora, G., Fung, H.C., Britton, A., Arepalli, S., *et al.* (2009) A two-stage genome-wide association study of sporadic amyotrophic lateral sclerosis. *Hum. Mol. Genet.*, **18**, 1524–1532.

11. Steinberg, K.M., Yu, B., Koboldt, D.C., Mardis, E.R. and Pamphlett, R. (2015) Exome sequencing of case-unaffected-parents trios reveals recessive and *de novo* genetic variants in sporadic ALS. *Sci. Rep.*, **5**, 9124.

12. Berridge, M.J. (1993) Inositol trisphosphate and calcium signalling. *Nature*, **361**, 315–325.

13. Yamamoto-Hino, M., Sugiyama, T., Hikichi, K., Mattei, M.G., Hasegawa, K., Sekine, S., Sakurada, K., Miyawaki, A., Furuichi, T., Hasegawa, M., *et al.* (1994) Cloning and characterization of human type 2 and type 3 inositol 1,4,5-trisphosphate receptors. *Receptors Channels*, **2**, 9–22.

14. Iwai, M., Tateishi, Y., Hattori, M., Mizutani, A., Nakamura, T., Futatsugi, A., Inoue, T., Furuichi, T., Michikawa, T. and Mikoshiba, K. (2005) Molecular cloning of mouse type 2 and type 3 inositol 1,4,5-trisphosphate receptors and identification of a novel type 2 receptor splice variant. *J. Biol. Chem.*, **280**, 10305–10317.

15. Sheppard, C.A., Simpson, P.B., Sharp, A.H., Nucifora, F.C., Ross, C.A., Lange, G.D. and Russell, J.T. (1997) Comparison of type 2 inositol 1,4,5-trisphosphate receptor distribution and subcellular Ca^{2+} release sites that support Ca^{2+} waves in cultured astrocytes. *J. Neurochem.*, **68**, 2317–2327.

16. Oberdorf, J., Vallano, M.L. and Wojcikiewicz, R.J. (1997) Expression and regulation of types I and II inositol 1,4,5-trisphosphate receptors in rat cerebellar granule cell preparations. *J. Neurochem.*, **69**, 1897–1903.

17. Sharp, A.H., Nucifora, F.C., Jr., Blondel, O., Sheppard, C.A., Zhang, C., Snyder, S.H., Russell, J.T., Ryugo, D.K. and Ross, C.A. (1999) Differential cellular expression of isoforms of inositol 1,4,5-triphosphate receptors in neurons and glia in brain. *J. Comp. Neurol.*, **406**, 207–220.

18. Zeisel, A., Munoz-Manchado, A.B., Codeluppi, S., Lonnerberg, P., La Manno, G., Jureus, A., Marques, S., Munguba, H., He, L., Betsholtz, C. *et al.* (2015) Brain structure. Cell types in the mouse cortex and hippocampus revealed by single-cell RNA-seq. *Science*, **347**, 1138–1142.

19. Martinez-Gomez, A. and Dent, M.A. (2007) Expression of IP_3 receptor isoforms at the nodes of Ranvier in rat sciatic nerve. *NeuroReport*, **18**, 447–450.

20. Sugiyama, T., Furuya, A., Monkawa, T., Yamamoto-Hino, M., Satoh, S., Ohmori, K., Miyawaki, A., Hanai, N., Mikoshiba, K. and Hasegawa, M. (1994) Monoclonal antibodies distinctively recognizing the subtypes of inositol 1,4,5-trisphosphate receptor: application to the studies on inflammatory cells. *FEBS Lett.*, **354**, 149–154.

21. Petravicz, J., Fiacco, T.A. and McCarthy, K.D. (2008) Loss of IP_3 receptor-dependent Ca^{2+} increases in hippocampal astrocytes does not affect baseline CA1 pyramidal neuron synaptic activity. *J. Neurosci.*, **28**, 4967–4973.

22. Agulhon, C., Fiacco, T.A. and McCarthy, K.D. (2010) Hippocampal short- and long-term plasticity are not modulated by astrocyte Ca^{2+} signaling. *Science*, **327**, 1250–1254.

23. Takata, N., Mishima, T., Hisatsune, C., Nagai, T., Ebisui, E., Mikoshiba, K. and Hirase, H. (2011) Astrocyte calcium signaling transforms cholinergic modulation to cortical plasticity *in vivo*. *J. Neurosci.*, **31**, 18155–18165.

24. Futatsugi, A., Nakamura, T., Yamada, M.K., Ebisui, E., Nakamura, K., Uchida, K., Kitaguchi, T., Takahashi-Iwanaga, H., Noda, T., Aruga, J., *et al.* (2005) IP_3 receptor types 2 and 3 mediate exocrine secretion underlying energy metabolism. *Science*, **309**, 2232–2234.

25. Van Den Bosch, L., Van Damme, P., Bogaert, E. and Robberecht, W. (2006) The role of excitotoxicity in the pathogenesis of amyotrophic lateral sclerosis. *Biochim. Biophys. Acta*, **1762**, 1068–1082.

26. Van Den Bosch, L., Vandenberghe, W., Klaassen, H., Van Houtte, E. and Robberecht, W. (2000) Ca^{2+}-permeable AMPA receptors and selective vulnerability of motor neurons. *J. Neurol. Sci.*, **180**, 29–34.

27. Staats, K.A., Bogaert, E., Hersmus, N., Jaspers, T., Luyten, T., Bultynck, G., Parys, J.B., Hisatsune, C., Mikoshiba, K., Van Damme, P., *et al.* (2012) Neuronal overexpression of IP_3 receptor 2 is detrimental in mutant SOD1 mice. *Biochem. Biophys. Res. Commun.*, **429**, 210–213.

28. Staats, K.A., Van Helleputte, L., Jones, A.R., Bento-Abreu, A., Van Hoecke, A., Shatunov, A., Simpson, C.L., Lemmens, R., Jaspers, T., Fukami, K., *et al.* (2013) Genetic ablation of phospholipase C delta 1 increases survival in SOD1^{G93A} mice. *Neurobiol. Dis.*, **60**, 11–17.

29. Tadic, V., Prell, T., Lautenschlaeger, J. and Grosskreutz, J. (2014) The ER mitochondria calcium cycle and ER stress response as therapeutic targets in amyotrophic lateral sclerosis. *Front. Cell. Neurosci.*, **8**, 147.

30. Grosskreutz, J., Van Den Bosch, L. and Keller, B.U. (2010) Calcium dysregulation in amyotrophic lateral sclerosis. *Cell Calcium*, **47**, 165–174.
31. Fukuda, N., Shirasu, M., Sato, K., Ebisui, E., Touhara, K. and Mikoshiba, K. (2008) Decreased olfactory mucus secretion and nasal abnormality in mice lacking type 2 and type 3 IP_3 receptors. *Eur. J. Neurosci.*, **27**, 2665–2675.
32. Uchida, K., Aramaki, M., Nakazawa, M., Yamagishi, C., Makino, S., Fukuda, K., Nakamura, T., Takahashi, T., Mikoshiba, K. and Yamagishi, H. (2010) Gene knock-outs of inositol 1,4,5-trisphosphate receptors types 1 and 2 result in perturbation of cardiogenesis. *PLoS One*, **5**, e12500.
33. Klar, J., Hisatsune, C., Baig, S.M., Tariq, M., Johansson, A.C., Rasool, M., Malik, N.A., Ameur, A., Sugiura, K., Feuk, L., *et al.* (2014) Abolished InsP$_3$R2 function inhibits sweat secretion in both humans and mice. *J. Clin. Invest.*, **124**, 4773–4780.
34. Viswanathan, K., Liu, L., Vaziri, S., Dai, E., Richardson, J., Togonu-Bickersteth, B., Vatsya, P., Christov, A. and Lucas, A.R. (2006) Myxoma viral serpin, Serp-1, a unique interceptor of coagulation and innate immune pathways. *Thromb. Haemost.*, **95**, 499–510.
35. Byrnes, K.R., Stoica, B., Loane, D.J., Riccio, A., Davis, M.I. and Faden, A.I. (2009) Metabotropic glutamate receptor 5 activation inhibits microglial associated inflammation and neurotoxicity. *Glia*, **57**, 550–560.
36. Anneser, J.M., Chahli, C., Ince, P.G., Borasio, G.D. and Shaw, P.J. (2004) Glial proliferation and metabotropic glutamate receptor expression in amyotrophic lateral sclerosis. *J. Neuropathol. Exp. Neurol.*, **63**, 831–840.
37. Aronica, E., Catania, M.V., Geurts, J., Yankaya, B. and Troost, D. (2001) Immunohistochemical localization of group I and II metabotropic glutamate receptors in control and amyotrophic lateral sclerosis human spinal cord: upregulation in reactive astrocytes. *Neuroscience*, **105**, 509–520.
38. Geurts, J.J., Wolswijk, G., Bo, L., van der Valk, P., Polman, C.H., Troost, D. and Aronica, E. (2003) Altered expression patterns of group I and II metabotropic glutamate receptors in multiple sclerosis. *Brain*, **126**, 1755–1766.
39. Stanimirovic, D.B., Ball, R., Mealing, G., Morley, P. and Durkin, J.P. (1995) The role of intracellular calcium and protein kinase C in endothelin-stimulated proliferation of rat type I astrocytes. *Glia*, **15**, 119–130.
40. Floyd, C.L., Rzigalinski, B.A., Sitterding, H.A., Willoughby, K.A. and Ellis, E.F. (2004) Antagonism of group I metabotropic glutamate receptors and PLC attenuates increases in inositol trisphosphate and reduces reactive gliosis in strain-injured astrocytes. *J. Neurotrauma*, **21**, 205–216.
41. Strokin, M., Sergeeva, M. and Reiser, G. (2011) Proinflammatory treatment of astrocytes with lipopolysaccharide results in augmented Ca^{2+} signaling through increased expression of via phospholipase A2 (iPLA2). *Am. J. Physiol. Cell. Physiol.*, **300**, C542–C549.
42. Leon, C.M., Barbosa, C.M., Justo, G.Z., Borelli, P., Resende, J.D.J., Oliveira, J.S., Ferreira, A.T. and Paredes-Gamero, E.J. (2011) Requirement for PLC γ 2 in IL-3 and GM-CSF-stimulated MEK/ERK phosphorylation in murine and human hematopoietic stem/progenitor cells. *J. Cell. Physiol.*, **226**, 1780–1792.
43. Shytle, R.D., Mori, T., Townsend, K., Vendrame, M., Sun, N., Zeng, J., Ehrhart, J., Silver, A.A., Sanberg, P.R. and Tan, J. (2004) Cholinergic modulation of microglial activation by alpha 7 nicotinic receptors. *J. Neurochem.*, **89**, 337–343.
44. Suzuki, T., Hide, I., Matsubara, A., Hama, C., Harada, K., Miyano, K., Andra, M., Matsubayashi, H., Sakai, N., Kohsaka, S., *et al.* (2006) Microglial alpha7 nicotinic acetylcholine receptors drive a phospholipase C/IP3 pathway and modulate the cell activation toward a neuroprotective role. *J. Neurosci. Res.*, **83**, 1461–1470.
45. Bagayogo, I.P. and Dreyfus, C.F. (2009) Regulated release of BDNF by cortical oligodendrocytes is mediated through metabotropic glutamate receptors and the PLC pathway. *ASN Neuro*, **1**, e00001.
46. Blanchet, M.R., Israel-Assayag, E., Daleau, P., Beaulieu, M.J. and Cormier, Y. (2006) Dimethyphenylpiperazinium, a nicotinic receptor agonist, downregulates inflammation in monocytes/macrophages through PI3K and PLC chronic activation. *Am. J. Physiol. Lung Cell. Mol. Physiol.*, **291**, L757–L763.
47. Lomakina, E.B. and Waugh, R.E. (2010) Signaling and dynamics of activation of LFA-1 and Mac-1 by immobilized IL-8. *Cell. Mol. Bioeng.*, **3**, 106–116.
48. Hunter, I., Mascall, K.S., Ramos, J.W. and Nixon, G.F. (2011) A phospholipase C{gamma}1-activated pathway regulates transcription in human vascular smooth muscle cells. *Cardiovasc. Res.*, **90**, 557–564.
49. Teuling, E., van Dis, V., Wulf, P.S., Haasdijk, E.D., Akhmanova, A., Hoogenraad, C.C. and Jaarsma, D. (2008) A novel mouse model with impaired dynein/dynactin function develops amyotrophic lateral sclerosis (ALS)-like features in motor neurons and improves lifespan in SOD1-ALS mice. *Hum. Mol. Genet.*, **17**, 2849–2862.
50. Lemmens, R., Jaspers, T., Robberecht, W. and Thijs, V.N. (2013) Modifying expression of EphA4 and its downstream targets improves functional recovery after stroke. *Hum. Mol. Genet.*, **22**, 2214–2220.
51. Fischer, L.R., Culver, D.G., Tennant, P., Davis, A.A., Wang, M., Castellano-Sanchez, A., Khan, J., Polak, M.A. and Glass, J.D. (2004) Amyotrophic lateral sclerosis is a distal axonopathy: evidence in mice and man. *Exp. Neurol.*, **185**, 232–240.